PCCP

RSC Publishing

PAPER

View Article Online
View Journal | View Issue

Published on 27 September 2013. Downloaded by University of Tennessee at Knoxville on 23/12/2015 15:34:36.

Cite this: *Phys. Chem. Chem. Phys.*, 2013, **15**, 19496

Correlating cation ordering and voltage fade in a lithium–manganese-rich lithium-ion battery cathode oxide: a joint magnetic susceptibility and TEM study†

Debasish Mohanty,*[a] Athena S. Sefat,[a] Jianlin Li,[b] Roberta A. Meisner,[a] Adam J. Rondinone,[c] E. Andrew Payzant,[d] Daniel P. Abraham,[e] David L. Wood III[bf] and Claus Daniel*[bf]

Structure–electrochemical property correlation is presented for lithium–manganese-rich layered–layered nickel manganese cobalt oxide (LMR–NMC) having composition $Li_{1.2}Co_{0.1}Mn_{0.55}Ni_{0.15}O_2$ (TODA HE5050) in order to examine the possible reasons for voltage fade during short-to-mid-term electrochemical cycling. The $Li_{1.2}Co_{0.1}Mn_{0.55}Ni_{0.15}O_2$ based cathodes were cycled at two different upper cutoff voltages (UCV), 4.2 V and 4.8 V, for 1, 10, and 125 cycles; voltage fade was observed after 10 and 125 cycles only when the UCV was 4.8 V. Magnetic susceptibility and selected-area electron diffraction data showed the presence of cation ordering in the pristine material, which remained after 125 cycles when the UCV was 4.2 V. When cycled at 4.8 V, the magnetic susceptibility results showed the suppression of cation ordering after one cycle; the cation ordering diminished upon further cycling and was not observed after 125 cycles. Selected-area electron diffraction data from oxides oriented towards the [0001] zone axis revealed a decrease in the intensity of cation-ordering reflections after one cycle and an introduction of spinel-type reflections after 10 cycles at 4.8 V; after 125 cycles, only the spinel-type reflections and the fundamental O3 layered oxide reflections were observed. A significant decrease in the effective magnetic moment of the compound after one cycle at 4.8 V indicated the presence of lithium and/or oxygen vacancies; analysis showed a reduction of Mn^{4+} (high spin/low spin) in the pristine oxide to Mn^{3+} (low spin) after one cycle. The effective magnetic moment was higher after 10 and 125 cycles at 4.8 V, suggesting the presence of Mn^{3+} in a high spin state, which is believed to originate from distorted spinel ($Li_2Mn_2O_4$) and/or spinel ($LiMn_2O_4$) compounds. The increase in effective magnetic moments was not observed when the oxide was cycled at 4.2 V, indicating the stability of the structure under these conditions. This study shows that structural rearrangements in the LMR–NMC oxide happen only at higher potentials (4.8 V, for example) and provides evidence of a direct correlation between cation ordering and voltage fade.

Received 29th August 2013,
Accepted 27th September 2013

DOI: 10.1039/c3cp53658k

www.rsc.org/pccp

Introduction

Rechargeable lithium ion batteries (LIBs) are promising energy storage devices for plug-in hybrid electric vehicles (PHEVs) and all-electric vehicles (EVs).[1–3] For these LIBs to become practical for transportation applications, a high-energy-density cathode (positive electrode) that is both safe and cost-effective is needed.[1] To meet these needs, the LIB research community has invested extensive effort in discovering new cathode materials with superior electrochemical performance, and diagnosing the problems with existing cathode materials for understanding the mechanisms that govern their life and safety.[4–6] Several years ago, Thackeray and co-workers proposed lithium–manganese-rich layered–layered nickel manganese cobalt oxides (LMR–NMCs) and identified those materials as promising candidates for

[a] *Materials Science and Technology Division, Oak Ridge National Laboratory, Oak Ridge, TN 37931, USA. E-mail: mohantyd@ornl.gov*
[b] *Energy and Transportation Science Division, Oak Ridge National Laboratory, Oak Ridge, TN 37831, USA*
[c] *Center for Nanophase Materials Sciences, Oak Ridge National Laboratory, Oak Ridge, TN 37931, USA*
[d] *Chemical and Engineering Materials Division, Oak Ridge National Laboratory, Oak Ridge, TN 37831, USA*
[e] *Chemical Sciences and Engineering Division, Argonne National Laboratory, Argonne, Illinois 60439, USA*
[f] *Bredesen Center for Interdisciplinary Research and Graduate Education, University of Tennessee, Knoxville, TN 37996, USA. E-mail: danielc@ornl.gov*

† Electronic supplementary information (ESI) available. See DOI: 10.1039/c3cp53658k

This journal is © the Owner Societies 2013

Published on 27 September 2013. Downloaded by University of Tennessee at Knoxville on 23/12/2015 15:34:36.

LIB EV applications.[7,8] These oxides, also denoted as xLiMO$_2$–$(1-x)$Li$_2$MnO$_3$ (M = Co, Mn, Ni), display cation ordering in the transition metal layer. The uniqueness of LMR–NMCs lies in their high voltage and high capacity, the latter being theoretically more than 250 A h kg^{-1} with a corresponding energy density of 900 W h kg^{-1} when charging beyond 4.5 V *vs.* Li$^+$/Li.[9] Recently, however, several research groups have observed major issues such as high first-cycle irreversible capacity loss,[10,11] impedance rise during high-voltage hold,[12] and voltage fade[9,13,14] during subsequent charge–discharge cycles. Several studies have been initiated to understand and resolve these issues; however, an understanding of "voltage fade" remains elusive in the LMR–NMC oxides.[10,11,15] When a LIB containing LMR–NMC cathode undergoes several charge–discharge cycles, the discharge voltage plateau shifts toward a lower profile, which is termed as voltage-fade. Such a dramatic shift in voltage profile is undesirable for automotive applications as it continuously alters the state of charge (SOC) calibration, and, hence, the predicted power and energy requirements at any operating SOC. The voltage fade phenomenon apparently results from structural changes/phase transformations in the oxide as reported by Gallagher *et al.*,[16] Croy *et al.*,[14] and Abraham *et al.*[9] *In situ* X-ray diffraction (XRD) also showed that a "layer to spinel-like" phase transformation could occur in the LMR–NMC cathode during repeated charge–discharge cycles, causing a depression in the voltage profile.[17]

The structure of the LMR–NMC compound is a composite[18,19] between the layered rhombohedral/trigonal (R$\bar{3}m$, or O3) phase and monoclinic ($C2/m$) crystal unit cells (Fig. 1). Unlike the stoichiometric LiCoO$_2$ structure, LMR–NMC oxides contain lithium atoms in the transition metal (TM) layer, which introduces Li-TM "cation ordering" resulting in LiMn$_6$ regions that are the building blocks of Li$_2$MnO$_3$.[20] The presence of cation ordering is confirmed by the ordering peaks that appear in the low two-theta region in an XRD pattern and by the superlattice-like reflections between two O3 fundamental reflections in selected-area electron diffraction obtained along the [0001] zone axis.[12] It is widely accepted that this cation ordering (Li$_2$MnO$_3$-like regions) plays an important role in delivering high capacities during cycling at high voltages (>4.5 V). Previous reports show that the degree of cation ordering decreases during first-cycle charging beyond 4.5 V because such charging induces an irreversible activation of the Li$_2$MnO$_3$ with possible release of oxygen.[21] This release of oxygen may change the oxidation states of TM ions. However, until now, there have been no reports that track the cation ordering and change in oxidation states of TM ions as a function of cycle numbers at different upper cut-off (UCV) voltages; hence, the relationship between cation ordering and voltage fade is unclear. An important reason is the inability to detect the less-intense cation-ordering peaks in XRD data after the initial (first) cycles.

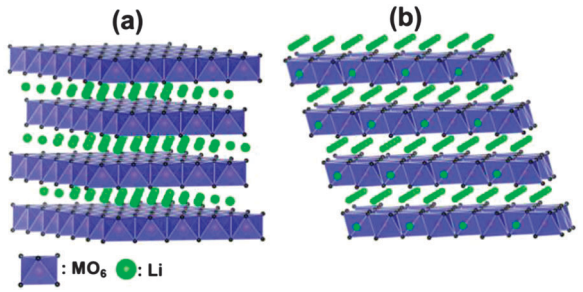

Fig. 1 Structure of the TODA HE5050 cathode, which is the integrated structure of layered trigonal (a) and layered monoclinic (b). The layered monoclinic phase contained Li in the TM layer, which induces cation ordering in the structure.

In this report, the approach is to employ magnetic susceptibility and transmission electron microscopy (TEM) as diagnostic tools to investigate the cation ordering in Li$_{1.2}$Co$_{0.1}$Mn$_{0.55}$Ni$_{0.15}$O$_2$ (TODA HE5050) after repeated charge–discharge cycles at two different cutoff voltages (4.2 and 4.8 V), and to correlate the cation ordering with voltage fade. The magnetic susceptibility measurement is more sensitive to cation ordering than XRD; TEM can provide the crystallographic (phase) information and oxidation states (TEM/electron energy loss spectrometry or EELS) from an individual crystal, which could be missed by XRD. Additionally, the magnetic susceptibility technique provides the bulk oxidation states of TM ions after repeated charge–discharge cycles; by using these two techniques, one can obtain the necessary structural information for investigating different redox reactions over subsequent charge–discharge cycles. Therefore, the objective of this work is to correlate the information obtained from magnetic susceptibility and TEM tools for understanding the voltage-fading phenomena in the LMR–NMC cathode oxide. Specific questions to be answered are: (1) is the voltage fade phenomenon dependent on upper cutoff voltage (UCV)? (2) Is there any correlation between cation ordering and voltage fade in LMR–NMC compounds? (3) What are the electronic states of TM ions after charge–discharge cycles? (4) How are these electronic state changes related to the voltage-fade process in LMR–NMC oxides?

Experimental section

The HE5050 LMR–NMC was synthesized by TODA America, Inc., and the electrodes were fabricated at the U.S. Department of Energy (DOE) Cell Fabrication Facility at Argonne National Laboratory. The composition and particle morphology of electrodes can be found in previous reports.[9,12,17,22] Briefly, the electrodes contain 86 wt% HE5050, 8 wt% Solvay 5130 PVDF binder, 4 wt% SFG-6 graphite (Timcal), and 2 wt% Super P®Carbon Black (Timcal). Half coin cells were assembled by using a 12 mm diameter disk of HE5050 as the cathode and lithium metal as the anode (∅12 mm diameter disk) with a Celgard 2325 separator (19 mm diam) and a 1.2 M solution of LiPF$_6$ in EC : EMC (3 : 7 ratio by weight) as the electrolyte (Purolyte®). Electrochemical cycling was carried out by using a BioLogic SP-200 potentiostat controlled using EC-Lab software (V. 10.02). Two sets of experiments were carried out; in one set, the UCV was set to 4.2 V (2.4–4.2 V voltage window) and in the other set, the UCV was set to 4.8 V (2.4–4.8 V voltage window). After completing 1, 10, and 125 cycles at 4.2 V and 4.8 V, the cells were allowed to rest for 6 h to attain the electrode stability (relaxed structure); the discharged cells were

Published on 27 September 2013. Downloaded by University of Tennessee at Knoxville on 23/12/2015 15:34:36.

Table 1 Sample identification for the study

Sample	Cutoff voltage	Cycles
LMR–NMC-4.8-1	4.8	1
LMR–NMC-4.8-10	4.8	10
LMR–NMC-4.8-125	4.8	125
LMR–NMC-4.2-1	4.2	1
LMR–NMC-4.2-10	4.2	10
LMR–NMC-4.2-125	4.2	125

then disassembled in a glove box with argon atmosphere. The cycled cathodes were harvested, washed several times with dimethyl carbonate (DMC), and stored in a glove box overnight to dry. The sample names used in this paper and their descriptions are summarized in Table 1.

A PANalytical X'Pert Pro system with a molybdenum source (λ = 0.76 Å) and automatic divergence and anti-scatter slits operated at 60 kV and 45 mA was used to collect XRD patterns from the pristine and cycled electrodes. A Hitachi HF3300 TEM at 300 kV was used to collect high-resolution TEM images and selected-area electron diffraction (SAED) patterns. The electron energy loss spectroscopy (EELS) data were collected using a Zeiss Libra 120 TEM at 130 kV. TEM specimens were prepared by removing the powder from the electrode and then gently grinding the powder, dispersing it in ethanol, and sonicating it for 10 to 15 min. A few drops of the solution were added to a holey Cu grid for TEM observation. Direct current (DC) magnetization was measured as a function of temperature, using a Quantum Design Magnetic Property Measurement System. Each sample was first cooled to 5 K at zero field. Then a field of 100 Oe was applied, and the data were collected from 5 K to 300 K [zero field cooling mode (ZFC)]. The sample was also cooled in the applied field from 300 K down to 5 K, while magnetization was measured [field cooling (FC)]. The effective magnetic moments were calculated from the molar mass of the active material (TODA HE5050).

The lattice constants of the compounds were obtained using the Rietveld method; X-pert HighScore Plus with zero sample displacement errors and available background correction was used to refine the collected XRD patterns. For the refinement, the unit cell of the layered $LiMO_2$ phase with the $R\bar{3}m$ space group and the Li_2MnO_3 phase with the $C2/m$ space group were considered. SAEDs were simulated using Desktop Microscopist software[28] by using the unit cell of $LiMO_2$ structure with the $R\bar{3}m$ space group and Li_2MnO_3 with the $C2/m$ space group; and spinel structure with the $Fd\bar{3}m$ space group as reported elsewhere.[12] Fast Fourier transforms (FFTs) were collected from the high-resolution TEM images and reflections were indexed based on the same procedure adopted for indexing the SAED patterns.

Results

Electrochemical results

Fig. 2a and b show the voltage *vs.* capacity plots from the cell containing LMR–NMC cathodes cycled at two different UCVs,

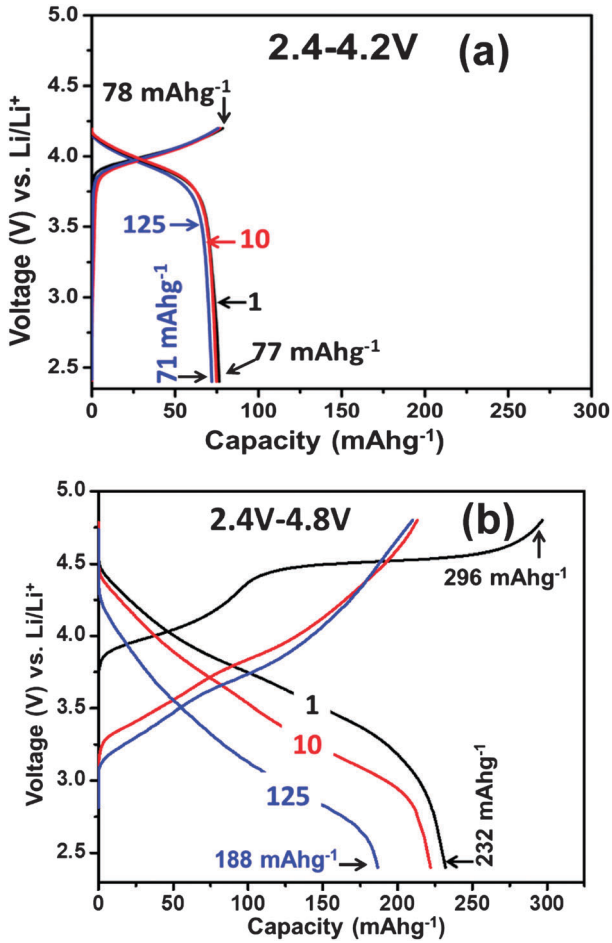

Fig. 2 The electrochemical voltage–capacity profiles from the cells cycled for 1, 10, and 125 times at cutoff voltage of (a) 4.2 V, and (b) 4.8 V. Voltage-fade was observed in Fig. 2b.

Table 2 *c*- and *a*-lattice parameters of pristine and cycled materials with charge and discharge capacities. The calculated error in the values is ≤1%

Materials (discharged state)	*c* (Å)	*a* (Å)	Charging capacity (mA h g^{-1})	Discharging capacity (mA h g^{-1})
LMR–NMC pristine	14.17	2.85		
LMR–NMC-4.2-1	14.19	2.84	78	77
LMR–NMC-4.2-10	14.20	2.84	77	75
LMR–NMC-4.2-125	14.20	2.84	74	71
LMR–NMC-4.8-1	14.22	2.83	296	232
LMR–NMC-4.8-10	14.29	2.83	232	224
LMR–NMC-4.8-125	14.34	2.86	195	188

4.2 V and 4.8 V, respectively, and the charge and discharge capacities are given in Table 2. When cycled at a 4.2 V UCV, the cell showed a first-cycle charging capacity of 78 mA h g^{-1} and a corresponding discharge capacity of 77 mA h g^{-1} with a ~98.7% Columbic efficiency. Good capacity retention is observed after subsequent 10 and 125 cycles (71 mA h g^{-1} after 125 cycles, 92% retention) showing a minor capacity fade, 0.06% per cycle. However, when the UCV is 4.8 V, the first-cycle charge and discharge capacities are 296 mA h g^{-1} and 232 mA h g^{-1}, respectively, much higher than those observed at a cutoff voltage

 This journal is © the Owner Societies 2013

Published on 27 September 2013. Downloaded by University of Tennessee at Knoxville on 23/12/2015 15:34:36.

of 4.2 V. However, at the 4.8 V cutoff voltage, a first-cycle irreversible capacity loss of ~64 mA h g^{-1} is observed, which is similar to that reported in the literature.[13] The discharge capacities on further cycling are 224 mA h g^{-1} after 10 cycles, and 188 mA h g^{-1} after 125 cycles. Capacity retention after 125 cycles is ~82%, corresponding to 0.15% capacity fade per cycle higher than that observed for 4.2 V UCV. In addition, the charge–discharge voltage plateau shifts to a lower profile in Fig. 2b, which becomes more pronounced with increasing cycle number indicating voltage-fade. The electrochemistry data can be summarized as follows. Cycling in the 2.4–4.2 V window yields (1) discharge capacity <80 mA h g^{-1} in the first cycle; (2) negligible irreversible capacity loss in the first charge–discharge cycle; and (3) no voltage-fade and minor capacity-fade through 125 cycles. In contrast, cycling in the 2.4–4.8 V window yields (1) discharge capacity >230 mA h g^{-1} obtained in the first cycle; (2) substantial irreversible capacity loss in the first charge–discharge cycle; and (3) capacity fade and significant voltage fade after 125 cycles. These data show that voltage fade occurs only when LMR–NMC samples are cycled at high voltages.

X-ray diffraction

The XRD plots of the LMR–NMC material in its pristine state and after 1, 10, and 125 cycles at cutoff voltages of 4.2 V and 4.8 V are shown in Fig. 3 and 4, respectively. All the major peaks in the pristine LMR–NMC powder (Fig. 3a or 4a) can be assigned to the rhombohedral or trigonal ($R\bar{3}m$ space group, represented as O3) phase except the less-intense extra peaks at lower 2-theta angles (marked in a dotted square), which can only be assigned to a monoclinic phase ($C2/m$ space group). These (extra) reflections in the XRD pattern from the pristine LMR–NMC material indicate the cation ordering between lithium and TM (Mn) ions in the TM layers and verify the presence of Li_2MnO_3-like regions, in agreement with previous reports.[7,13,23] After subsequent cycles

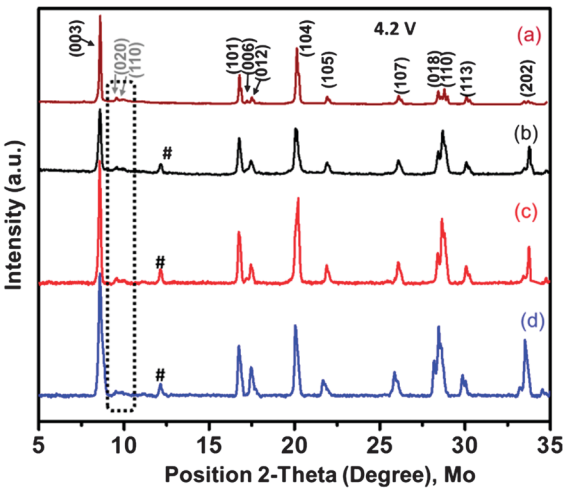

Fig. 3 XRD plots of LMR–NMC in the voltage window of 2.4–4.2 V showing trigonal/O_3 peaks as major peaks: (a) pristine, (b) after 1 cycle, (c) 10 cycles, and (d) 125 cycles. The cation-ordering peaks originating from Li_2MnO_3 phase are visible after 125 cycles (dotted rectangle). The # marker shows the peak obtained from graphitic carbon.

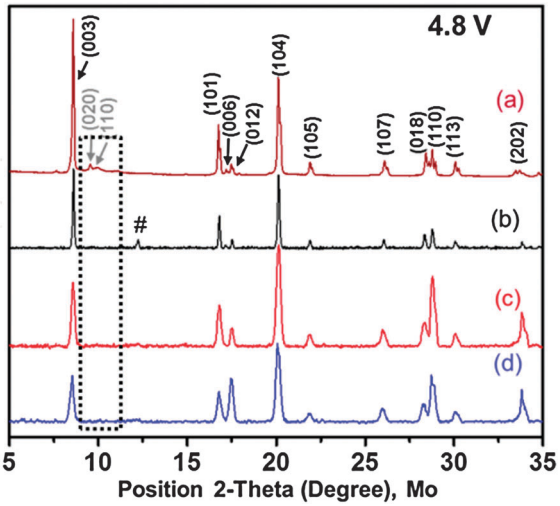

Fig. 4 XRD plots of LMR–NMC within the voltage window of 2.4–4.8 V showing trigonal/O_3 peaks as major peaks: (a) pristine, (b) after 1 cycle, (c) 10 cycles, and (d) 125 cycles. The cation-ordering peaks originating from Li_2MnO_3 phase are not observed after the initial cycles (dotted rectangle). The # marker shows the peak from graphitic carbon.

(regardless of the cutoff voltage), the O3 phase is retained in the structure until 125 cycles. Additionally, the cation-ordering peaks are present in all cycled samples when the UCV is 4.2 V; however, when the UCV is 4.8 V, these peaks are not seen, even after 1 cycle (see the highlighted regions in Fig. 3 and 4). The disappearance of these peaks is attributed to activation of the Li_2MnO_3 regions, and indicates the suppression of Li-TM ordering in the TM planes. The refined lattice parameters for the pristine and cycled oxide materials are presented in Table 2. The *c*- and *a*-lattice parameters for the LMR–NMC pristine material were calculated as 14.17 Å and 2.85 Å, respectively. After subsequent cycling at 4.2 V, the *c* lattice parameter increased to 14.20 Å, an increase of 0.15% as compared to the pristine oxide powder. When the cells are cycled at 4.8 V, the *c*-lattice parameter increases slightly and is greater than the value for the cycle at 4.2 V. The *c*-lattice parameter becomes more pronounced over 10 cycles (~0.8%) and 125 cycles (~1.2%) at 4.8 V. This increase is also in agreement with the (003) peak position in the XRD patterns (Fig. 5). The shift of (003) peaks toward lower 2-theta values when cycled at 4.8 V generally indicates the increase in $d_{(003)}$ and confirms the lattice expansion along the *c*-axis. However, when the cells are cycled at 4.2 V, no pronounced shift of the (003) peak toward lower 2-theta is observed, which clearly shows that larger lattice expansion occurs when cycling at 4.8 V UCV. The *a*-lattice parameters in the cycled samples decrease slightly initially, relative to the pristine sample, and then remain constant to 125 cycles for the 4.2 V UCV. However, when the UCV is 4.8 V, the *a* lattice parameter decreases after one cycle, then increases upon further cycling to 125 cycles. Closer examination shows that the ratio of (003) to (104) normalized intensity, $[I_{(003)}/I_{(104)}] > 1.2$ for the pristine HE5050 oxide, which indicates a layered structure as explained by Ohzuku *et al.*[24] For the oxides cycled at 4.2 V, the $I_{(003)}/I_{(104)}$ value remains greater than 1.2 indicating that the layered structure is preserved even after

Published on 27 September 2013. Downloaded by University of Tennessee at Knoxville on 23/12/2015 15:34:36.

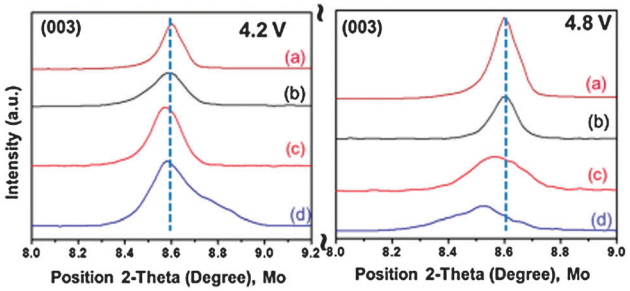

Fig. 5 The (003) peak positions for LMR–NMC when the cutoff voltage was 4.2 V (left) and 4.8 V (right): (a) pristine, (b) after 1 cycle, (c) after 10 cycles, and (d) after 125 cycles, and an (003) peak shift was observed when the cutoff voltage was 4.8 V.

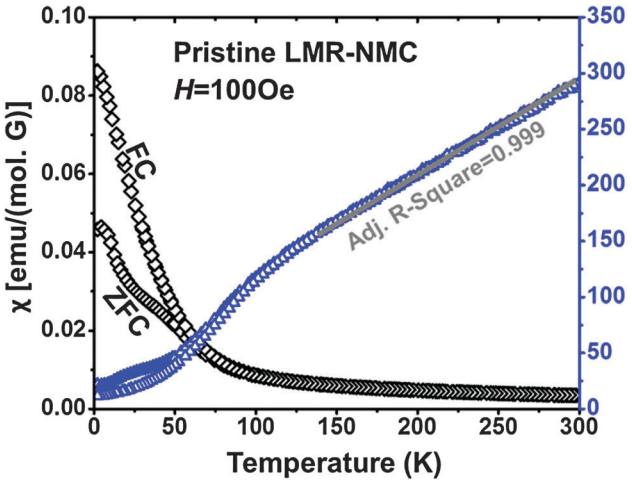

Fig. 6 Temperature dependence of the molar magnetic susceptibility of pristine LMR–NMC at 100 Oe showing bifurcation of the FC and ZFC curves at ~50 K, indicating magnetic ordering in the compound.[19] The variation of inverse magnetic susceptibility (FC and ZFC) and the Curie–Weiss fit is presented in the right *y*-axis.

125 charge–discharge cycles. However, when the UCV is 4.8 V, $I_{(003)}/I_{(104)} < 1.2$ after 125 cycles, which indicates a decrease in the layered character and/or increase in the spinel character of the oxide. Peak broadening is observed in the XRD plots after 125 cycles irrespective of the cutoff voltage. This peak broadening represents a decrease in the long-range coherency (increase in nano-domains) within the oxide particles. Moreover, slight increase in the (110) peak intensity was observed for some of the materials (regardless of UCV) after cycling which may be due to the overlap of the Al (current collector) and oxide peaks at a two theta of ~29° ((110) of HE5050 oxide and (220) of Al have nearly same *d*-spacing) or preferred orientation of (220) reflection from the Al current collector.

The XRD data/analysis can be summarized as follows. When cycled in the 2.4–4.2 voltage window: (1) the cation-ordering peaks are retained even after 125 cycles; and (2) a slight lattice expansion along the *c*-axis is observed. However, when cycled in the 2.4–4.8 V window: (1) the cation-ordering peaks are not seen after one (10/125) cycle(s); and (2) significant lattice expansion is observed along the *c*-axis.

Magnetic susceptibility

The temperature dependence of (inverse) molar magnetic susceptibility (χ^{-1}) χ with FC and ZFC for the pristine LMR–NMC material (electrode) is shown in Fig. 6. The pristine LMR–NMC material shows paramagnetic (PM) behaviour obeying the Curie–Weiss law at a temperature above ~100 K and an increase in magnetic susceptibility is observed in the low-temperature region (≤50 K).[19] The most important feature in the magnetic susceptibility curve that distinguishes these LMR–NMC compounds from the stoichiometric $LiMO_2$ ($LiCoO_2$ or $LiCo_{0.33}Mn_{0.33}Ni_{0.33}O_2$)[25] is the bifurcation (here, bifurcation is referred to as separation of FC and ZFC at ordering temperature) of the FC and ZFC curves at T_N = 50 K.[19] This feature indicates magnetic ordering in the LMR–NMC material, which is absent in the $LiMO_2$ compounds. The ordering in the LMR–NMC compound is generated exclusively from the Li_2MnO_3 component and confirms the presence of cation ordering.[12] In Li_2MnO_3, Mn^{4+} is a magnetic ion with d^3 configuration and shares the edges with another Mn^{4+} ion *via* oxygen in a 90° Mn^{4+}–O–Mn^{4+} interaction that is strongly antiferromagnetic (AFM). The temperature at which this ordering occurs [the Néel temperature (T_N)] is ~35 K.[26] The pristine LMR–NMC compound undergoes an magnetic ordering at 50 K (T_N = 50 K), which is slightly higher than the ordering temperature of pure Li_2MnO_3. This ordering may occur because the pristine LMR–NMC oxide has a mixture of phases [Li_2MnO_3 and $LiMO_2$ (M = Co, Mn, Ni)].[19]

The bifurcation of the FC and ZFC curves is an indication of cation ordering in LMR–NMC material and was monitored in the cycled samples. The oxidation states of the TM ions were determined by comparing the experimental effective magnetic moment with the calculated effective magnetic moment. The experimental effective magnetic moment was obtained from a linear fit in the plot of inverse molar magnetic susceptibility *vs.* temperature between 140 and 300 K (see Fig. 6) using equation $\chi_m = C_m(T - \theta)$, where χ_m is the molar magnetic susceptibility, C_m is the Curie constant and θ is the Curie–Weiss temperature. The calculated effective magnetic moment was obtained by considering the magnetic moments of Ni in the 2+, 3+, and 4+ states; Mn in the 3+, 4+, 5+, and 6+ states; and Co in the 3+ and 4+ states with both low spin (LS) and high spin (HS) configurations in an octahedral environment (TMO_6). The experimental effective magnetic moment for the pristine LMR–NMC compound was found to be 3.06 ± 0.02 μ_B and is comparable to the calculated effective magnetic moment with 0.15 mol of Ni^{2+} (S = 1), 0.55 mol of Mn^{4+} (S = 3/2), and 0.1 mol of Co^{3+} (S = 0).[12]

Hence the pristine LMR–NMC compound can be represented as $Li_{1.2}Co_{0.1}{}^{3+}Mn_{0.55}{}^{4+}Ni_{0.15}{}^{2+}O_2$ (Table 3).[12] The Curie–Weiss temperature for the pristine material was calculated to be −41 K. The negative value generally represents the AFM nature of the pristine material as reported elsewhere.[27]

LMR–NMC cycled at 4.2 V

Plots of the temperature dependence of the (inverse) molar magnetic susceptibility of the LMR–NMC samples cycled in the

 This journal is © the Owner Societies 2013

Published on 27 September 2013. Downloaded by University of Tennessee at Knoxville on 23/12/2015 15:34:36.

Table 3 The experimental effective magnetic moment, Curie–Weiss temperature, Néel temperature, and *f* values of pristine LMR–NMC and LMR–NMC materials cycled at 4.2 V and 4.8 V. The model shows the oxidation states of TM ions contributing to the experimental effective magnetic moment values

Sample	μ_{exp} (BM)	Model	θ (K)	T_N (K)	f
LMR–NMC	3.08 ± 0.01	$0.15Ni^{2+}$, $0.55Mn^{4+}$, $0.1Co^{3+}$	−41	50	0.82
4.2 V					
LMR–NMC-4.2-1	2.92 ± 0.02	Ni^{+3}, Ni^{2+}, Mn^{4+}, Co^{3+}	−48	50	0.96
LMR–NMC-4.2-10	2.93 ± 0.01	Ni^{+3}, Ni^{2+}, Mn^{4+}, Co^{3+}	−45	50	0.90
LMR–NMC-4.2-125	2.95 ± 0.04	Ni^{+3}, Ni^{2+}, Mn^{4+}, Co^{3+}	−46	50	0.92
4.8 V					
LMR–NMC-4.8-1	2.84 ± 0.01	Ni^{+3}, Ni^{2+}, Mn^{4+}, Co^{3+}, Mn^{3+}	−35	40	0.89
LMR–NMC-4.8-10	2.98 ± 0.02	Ni^{+3}, Ni^{2+}, Mn^{4+}, Co^{3+}, Mn^{3+}, Mn^{2+}	−30	30	1.0
LMR–NMC-4.8-125	3.13 ± 0.02	Ni^{+3}, Ni^{2}, Mn^{4+}, Co^{3+}, Mn^{3+}, Mn^{2+}	−19	10	1.9

voltage window of 2.4 to 4.2 V for 1, 10, and 125 cycles are presented in Fig. 7(a–c). The cycled materials show PM behaviour at $T \geq 100$ K and an increase in magnetic susceptibility was observed at $T \leq 50$ K. This observation is similar to the results obtained from the pristine LMR–NMC material. After one cycle, the bifurcation of FC and ZFC curves occurs at $T_N \sim 50$ K and this feature, which represents cation ordering, is retained even after 125 cycles (see S1 for an enlarged view of the $0 \leq T \leq 60$ K region in Fig. 7). The T_N value is 50 K for all the materials irrespective of the cycle numbers (Table 3). The oxidation states of the TM ions were calculated by following the method described earlier (see Table 3). The experimental effective magnetic moment for LMR–NMC-4.2V-1 is 2.92 μ_B, which is smaller than the value obtained for the pristine LMR–NMC material. The decrease in effective magnetic moment after one cycle indicates that the Ni^{4+} ions ($S = 0$) formed during charging at 4.2 V are not all reduced to Ni^{2+} ($S = 1$) during discharge in the 4.2–2.4 V window, and further indicates the possible existence of Ni^{3+} or Mn^{5+} ions (these ions have lower magnetic moment than Ni^{2+}, Co^{3+}, or Mn^{4+}). However, Mn^{5+} is not expected at 4.2 V, so residual Ni^{3+} is most likely present in the compound. The effective magnetic moment values remain unchanged over 125 cycles (Table 3). The Curie–Weiss temperature values are similar for all the cycled materials, which indicate that the AFM property is more likely retained after extended cycling.

LMR–NMC cycled at 4.8 V

The temperature dependence of (inverse) molar magnetic susceptibility of the LMR–NMC material cycled in the 2.4 to 4.8 voltage window is shown in Fig. 7(d–f). Similar to the pristine LMR–NMC, and LMR–NMC cycled at 4.2 V, all materials show PM behaviour at $T \geq 100$ K, and an increase in magnetic susceptibility when $T \leq 50$ K. The bifurcation of the FC and ZFC curves, which is a signature of cation ordering, is observed after the first cycle. This observation is in contrast to the XRD data (Fig. 4), in which the low-angle peaks are not observed after one cycle. The result indicates the sensitivity of the magnetic-susceptibility technique to detect cation ordering in the complex LMR–NMC materials. The bifurcation decreases on further cycling (see Fig. 7d and Fig. S1, ESI†). In Fig. 7(d–f), it can be seen that the degree of bifurcation of the FC and ZFC curves gradually decreases after 1, 10 cycles and ultimately that strong bifurcation (bifurcation similar to the pristine LMR–NMC material) is not observed after 125 cycles. However, a separation of FC and ZFC curves is observed at $T \sim 10$ K. That is, the cation ordering is significantly lower or non-existent after 125 cycles. Another interesting observation is that the T_N value decreases with increased cycling. The T_N after 1 cycle is 40 ± 2 K and decreases to 30 ± 2 K and 10 ± 2 K for 10 and 125 cycles, respectively.

The effective magnetic moment is 2.84 μ_B after one cycle, which is less than the value for the pristine LMR–NMC material. However, unlike the result for 4.2 V samples, the experimental effective magnetic moment at 4.8 V increases over the subsequent cycles. In fact, the value after 125 cycles is equal or slightly higher than that for the pristine material (Table 3). These facts suggest that the average metal ion oxidation states are different for 4.2 V and 4.8 V samples. The decrease in effective magnetic moment after the first 4.8 V cycle suggests the presence of magnetic ions with low effective magnetic moment values. The following magnetic ions could lower the magnetic moment: Co^{4+} (LS), Ni^{3+} (LS), Mn^{5+} or Ni^{4+} (HS/LS), and Mn^{3+} (LS) or Mn^{2+} (LS) (see Table S2, ESI† for the magnetic moment values). All of these ions have lower effective magnetic moment than those of Ni^{2+}, Co^{3+}, or Mn^{4+} that are present in the pristine compound. However, Co^{4+}, Ni^{4+}, and Mn^{5+} ions can be excluded from the model because discharge to 2.4 V should reduce all these ions. Hence, we speculate that (1) there is residual Ni^{3+} in the compound with lithium vacancies (for charge compensation); (2) there are Mn^{2+}/Mn^{3+} ions with either only oxygen vacancies or a combination of lithium and oxygen vacancies. At a UCV of 4.2 V, oxygen vacancies are not expected because oxygen evolution is only expected to start at ~4.4 V, and, hence, the decrease in the effective magnetic moment can be attributed to the presence of residual Ni^{3+} ions. At a UCV of 4.8 V, the effective magnetic moment after one cycle is 0.24 μ_B lower than the pristine material (compared to 0.16 when the cutoff voltage is 4.2 V). Oxygen vacancies are expected in the sample.

Upon further cycling at 4.8 V, the effective magnetic moment increases, and eventually becomes equal or slightly larger than that of the pristine LMR–NMC compound after 125 cycles. This increase can be explained by invoking the presence of Mn^{3+} and

Published on 27 September 2013. Downloaded by University of Tennessee at Knoxville on 23/12/2015 15:34:36.

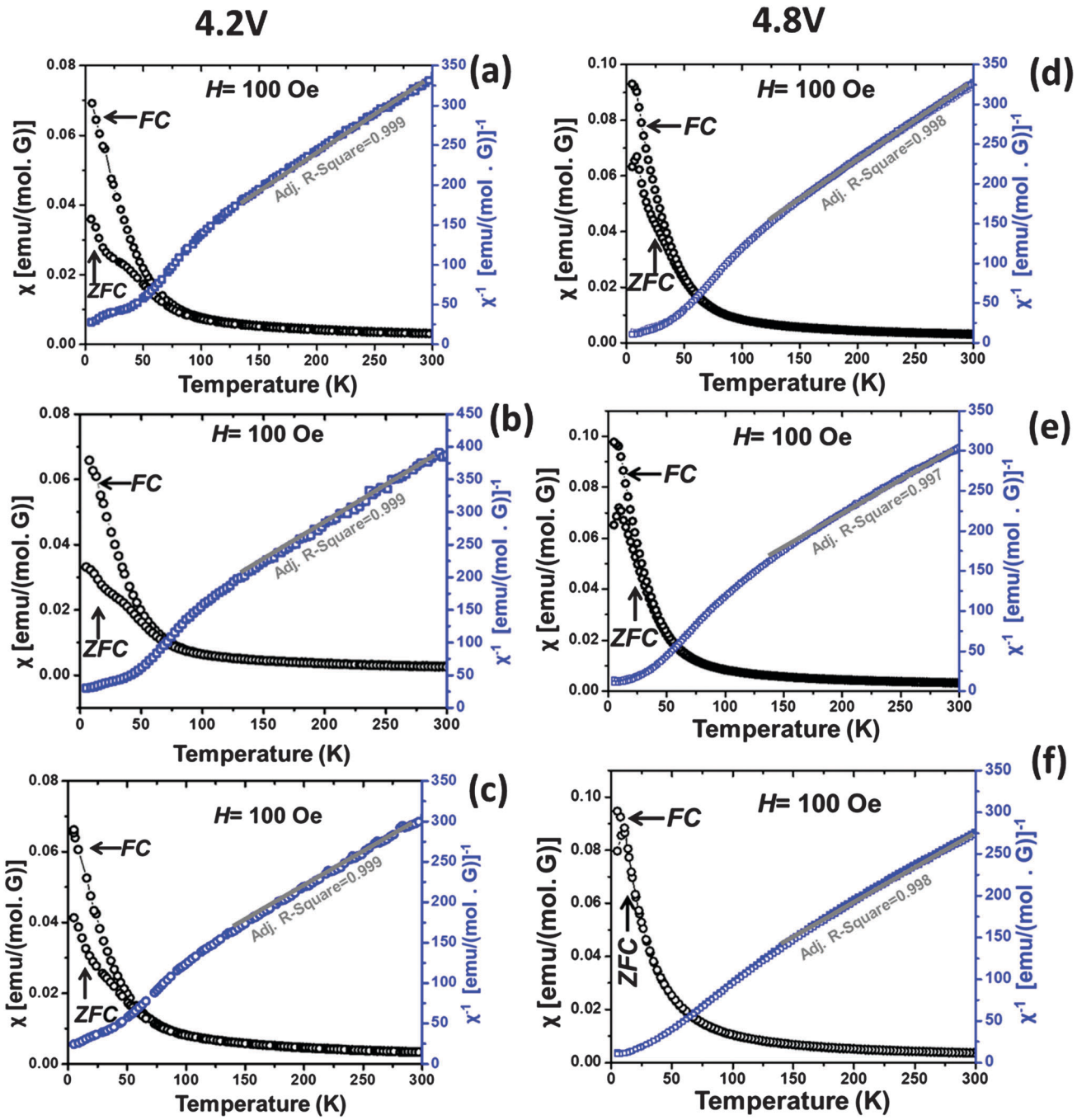

Fig. 7 Temperature dependence of the molar magnetic susceptibility of cycled LMR–NMC when cycled at a cutoff voltage 4.2 V ((a) after one cycle, (b) after 10 cycles, (c) after 125 cycles) and 4.8 V ((d) after one cycle, (e) after 10 cycle, (f) after 125 cycles). At 4.8 V, the cation ordering is suppressed as the cycle number increases. However, at 4.2 V, the ordering is retained until 125 cycles. The variation of inverse magnetic susceptibility (ZFC/FC) is shown on the right *y*-axis together with the Curie–Weiss fit.

Mn^{2+} in HS states. Because Mn^{2+} and Mn^{3+} have higher magnetic moments than Ni^{2+}, Mn^{4+}, and Co^{3+}, they can be formed at the expense of oxygen vacancies and lithium vacancies. The Curie–Weiss temperatures calculated for these materials are negative, which indicates retained AFM interaction in the compound. The fact that the values are less negative than those of samples cycled at 4.2 V indicates that the ferromagnetic interaction may have been introduced in the lattice during cycling at the higher UCV.

The magnetic susceptibility results can be summarized as follows. When cycled between 2.4 V and 4.2 V: (1) magnetic (cation) ordering is observed after one cycle, and is retained after 125 cycles; (2) the effective magnetic moment decreases slightly after one cycle, then remains almost unchanged after 10 and 125 cycles; (3) the T_N and Curie–Weiss temperature remained unchanged after cycling; and (4) analysis suggests that Ni^{3+} with lithium vacancies is present in the sample after the first cycle. When cycled between 2.4 and 4.8 V: (1) magnetic

 This journal is © the Owner Societies 2013

Published on 27 September 2013. Downloaded by University of Tennessee at Knoxville on 23/12/2015 15:34:36.

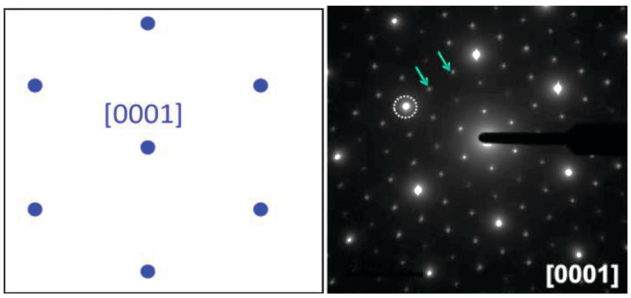

Fig. 8 The SAED pattern from the pristine LMR–NMC compound shows O3 as fundamental reflections (example: dotted circle) and the reflections showing cation ordering (indicated by the arrows).

(cation) ordering is observed after 1/10 cycles; however, the strength of the ordering is less than that for the pristine oxide; (2) after 125 cycles the ordering is not observed; (3) the effective magnetic moment decreases after one cycle, then increases during extended cycling (10/125 cycles); (4) T_N decreases with increasing cycle number; and (5) analysis suggests that Mn^{3+} and/or Mn^{2+} in HS states contribute to increasing the effective magnetic moment.

Transmission electron microscopy

SAED patterns were collected from several representative crystals. The crystals were oriented towards different zone axes (primarily [0001]) to monitor the cation-ordering reflections as a function of cycle numbers and cutoff voltage. The representative SAED pattern from a pristine LMR–NMC particle oriented along the [0001] zone axis is shown in Fig. 8. The bright fundamental reflection represents the O3 phase with trigonal symmetry.[28] The simulated SAED pattern along the [0001] zone axis is also presented in Fig. 8. The super reflections (marked with a solid arrow) in the experimental pattern indicate the cation ordering between Li and TM ions in the TM layers, forming a Li_2MnO_3-like phase, as explained in previous work.[29] A high-resolution TEM image from a representative particle is shown in Fig. 9a, and the corresponding FFT show the O3 and cation ordering reflections and simulated structures along the [0001] zone axis show the O3 reflections.

LMR–NMC cycled at 4.2 V

The representative SAED patterns, from particles cycled at 4.2 V, along the [0001] orientation are shown in Fig. 10a–c. In Fig. 10a, which shows the SAED patterns from LMR–NMC-4.2-1, cation-ordering reflections are observed after one cycle (indicated by arrow) and are retained after 10 and 125 cycles (Fig. 10b and c). The observed ordering reflections after 125 cycles (Fig. 10c) reveal that the Li_2MnO_3 like phase is still present in the structure, and that the LMR–NMC compound retains its original structure without undergoing major structure changes. The high-resolution TEM image in Fig. 9b of a LMR–NMC-4.2-125 particle shows the O3 type lattice, the corresponding FFT shows O3 along with cation ordering reflections; all are similar to the pristine LMR–NMC material (Fig. 9a). This observation is in agreement with the XRD and the magnetic susceptibility results, in which the ordering peaks (Fig. 3b–d) and bifurcation of FC and ZFC curves (Fig. 7a–c) are observed after 125 cycles.

LMR–NMC cycled at 4.8 V

Representative SAED patterns from particles cycled at 4.8 V are shown in Fig. 10d–f. Fig. 10d shows the SAED pattern from LMR–NMC-4.8-1 (after one cycle). A decrease in the intensity of ordering reflections is seen (see the intensity profile inset in Fig. 10d), which indicates that after the first cycle (where Li_2MnO_3 activation occurs), some cation ordering is still present in the structure. In Fig. 10e, the SAED pattern from representative particles of the LMR–NMC-4.8-10 sample (after 10 cycles) shows cation-ordering reflections. Additionally, new low intensity reflections are seen between the two fundamental O3 reflections. These new reflections are from a "spinel-like" phase[30] and arise from the presence of cations in tetrahedral sites of a spinel-type structure.[31] After 125 cycles (LMR–NMC-4.8-125), the Li-TM ordering reflections are absent, and particles with spinel reflections are observed along the [0001] zone axis. These spinel reflections were observed in 70% of the 25 oxide particles examined. The fundamental O3 reflections along the [0001] zone axis are also observed. To verify our findings, SAED patterns along the $[0\bar{1}11]$ zone axis were obtained from LMR–NMC particles cycled at 4.2 V and 4.8 V for 125 cycles. All reflections in the 4.2 V particles can be indexed by the O3 phase (see the simulated SAED pattern in Fig. 11). The arrow in the experimental SAED pattern indicates cation ordering in the structure originating from Li_2MnO_3 regions. The 4.8 V particles contain reflections corresponding to a spinel-phase (see the simulated SAED pattern in Fig. 11). The arrows in Fig. 11b show the reflections that are absent in the O3 phase. The high-resolution TEM image of the 4.8 V particles after 125 cycles shows a FFT pattern representative of a spinel structure (Fig. 9c), which is different from the results obtained from particles cycled at 4.2 V (Fig. 9b), where only O3 reflections are observed.

The results from the electron diffraction patterns can be summarized as follows. When cycled between 2.4 V and 4.2 V, the LMR–NMC particles retain cation-ordering reflections, indicating the presence of a significant amount of Li in the TM layers; the absence of new reflections after 125 cycles indicates that no major structural rearrangement occurs in the material. When cycled between 2.4 and 4.8 V, the intensity of cation-ordering peaks decreases after one cycle, a spinel-phase reflection is observed after 10 cycles; after 125 cycles, the cation-ordering peaks are not visible and the spinel-like reflections are stronger, which indicates a "layer to spinel" phase transformation.

Discussion

The pristine LMR–NMC compound has the composition $Li_{1.2}Co_{0.1}Mn_{0.55}Ni_{0.15}O_2$. The excess lithium creates ordering between the Li and TM ions (Mn) and forms a Li_2MnO_3-like phase. Cation-ordering peaks were observed in the XRD and SAED partners. In addition, the bifurcation of ZFC and FC

Published on 27 September 2013. Downloaded by University of Tennessee at Knoxville on 23/12/2015 15:34:36.

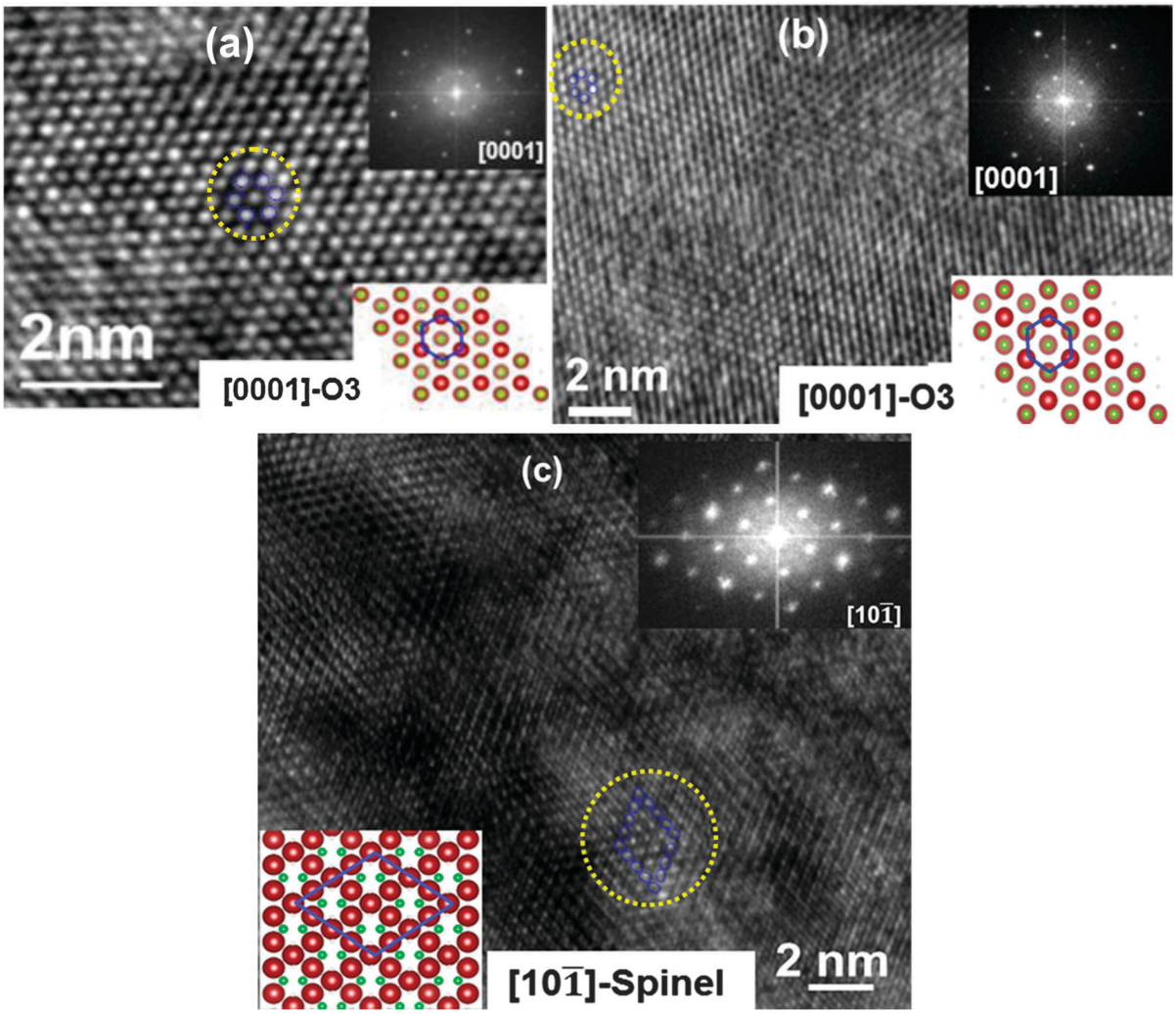

Fig. 9 High-resolution TEM images showing (a) the O3 phase in pristine LMR–NMC, (b) after 125 cycles to a cutoff voltage of 4.2 V, and (c) the spinel phase when cycled at cutoff voltage of 4.8 V. The corresponding FFT spot reflections: (a) and (b), O3; (c) spinel match with the simulated structures (insets) of O3 and spinel phase along [0001] and [10$\bar{1}$] zone axes. The highlighted regions in the experimental high-resolution TEM showing the atomic arrangements in O3 and spinel phases. The green and red atoms represent Li and TM (Mn/Co/Ni). The result is based on the observation from 25 particles.

(magnetic ordering) in the magnetic susceptibility data establishes that pristine LMR–NMC oxide structure can be described as an integrated structure of layered trigonal (SG 166, $R\bar{3}m$) and layered monoclinic (SG 12, $C2/m$) phases (Fig. 12a). When LMR–NMC is cycled in a 2.4–4.2 V window the achievable capacity is $\sim$77 mA h g^{-1} with no significant capacity fade and/or voltage fade over 125 cycles. However, when cycled in the 2.4–4.8 V voltage window, the discharge capacity is 242 mA h g^{-1} in the first cycle, with significant voltage and capacity fade in subsequent cycles indicating structural transformations in the material that need to be determined. When LMR–NMC is charged at 4.2 V, lithium ions are only extracted from the lithium layer; lithium ions are not extracted from the TM layer and Li-TM cation ordering is preserved (Fig. 12b). Charge-compensation for Li extraction results from the oxidation of Ni^{2+} to Ni^{4+}. During discharge, all lithium ions should ideally travel back to the lithium layer in the host oxide. However, the lower magnetic susceptibility of LMR–NMC-4.2-1 indicates that Ni^{3+} is present in the structure. The decrease in the *a*-lattice parameter also suggests that ions with lower ionic radii are present after the first discharge. Therefore, it appears that not all of the lithium ions extracted during first-cycle charging return to the host structure, and some vacancies remain in the lithium layer (Fig. 12c). Due to the presence of these vacancies, the repulsive force between cubic-closed-packed oxygen layers increases and slightly expands the structure along the *c*-axis, as seen from the increase in the *c*-lattice parameter after one cycle (Table 1). No further increase in the *c*-lattice parameter is observed for 125 cycles [see Table 1 and the (003) peak shift in Fig. 5a]. The appearance of cation ordering peaks in XRD plots and SAED patterns of LMR–NMC materials after 125 cycles at 4.2 V reveal that the Li_2MnO_3 regions are not fully activated during cycling. This result is confirmed by the magnetic-ordering feature (bifurcation of ZFC and FC curves) observed after 125 cycles. The data confirm that LMR–NMC is stable over 125 cycles in the 2.4–4.2 V voltage window.

 This journal is © the Owner Societies 2013

Published on 27 September 2013. Downloaded by University of Tennessee at Knoxville on 23/12/2015 15:34:36.

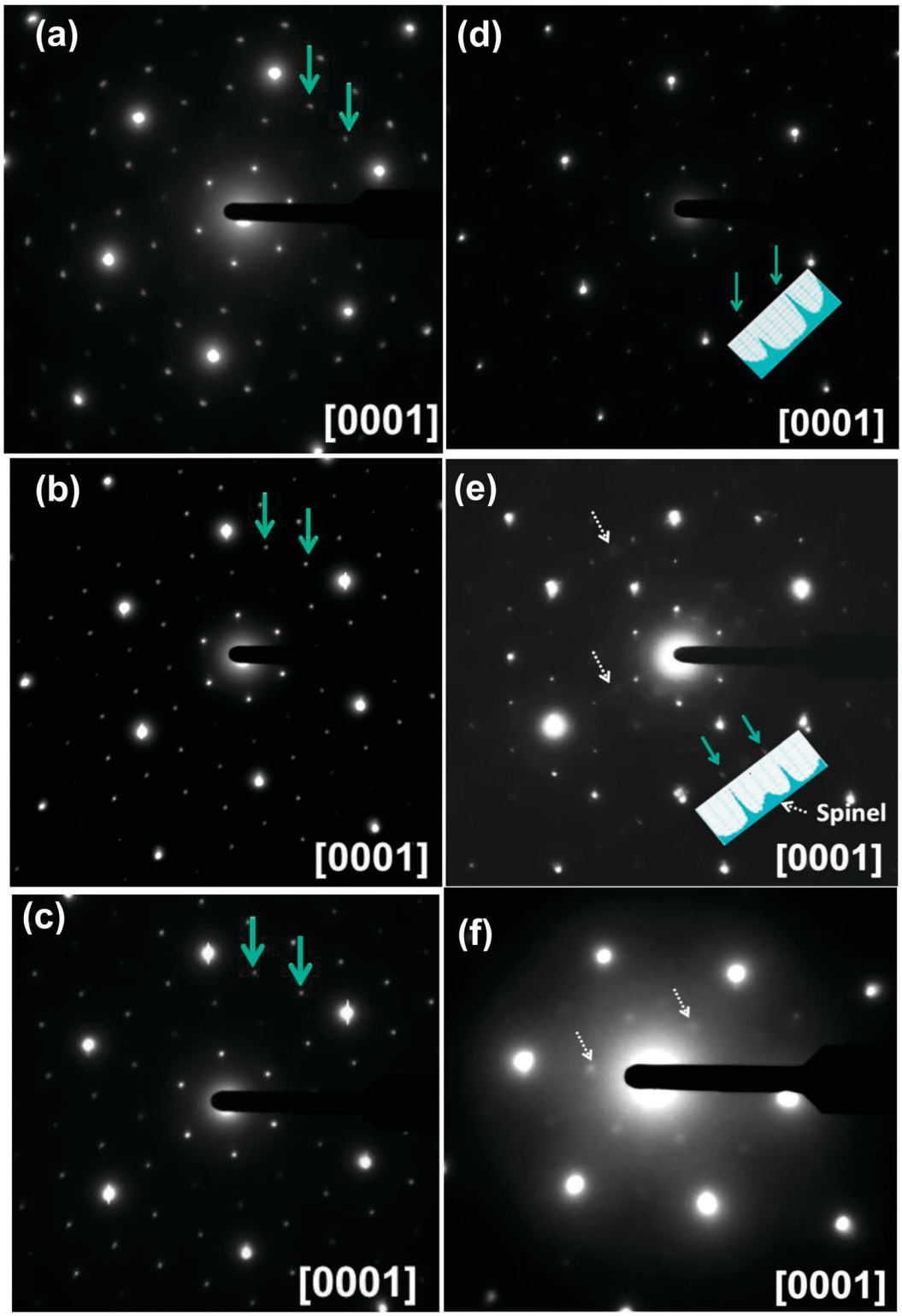

Fig. 10 Selected-area electron diffraction (SAED) images from particles cycled at a cutoff voltage of 4.2 V (left column): (a) after 1 cycle, (b) after 10 cycles, and (c) after 125 cycles and cycled at a cutoff voltage of 4.8 V (right column): (d) after 1 cycle, (e) after 10 cycles, and (f) after 125 cycles. The cation-ordering reflections were visible after 125 cycles when the cutoff voltage was 4.2 V [solid arrows in (a), (b), and (c)]. New spinel-type peaks were observed after 10 cycles when cutoff voltage was 4.8 V [dotted arrow in (e)]. (f) After 125 cycles at 4.8 V, the cation-ordering reflections were vanished, and only the spinel-type peaks were retained. The insets in (d) and (e) show the brightness profiles from the respective spots.

For the LMR–NMC cycled at 4.8 V, during charging the lithium ions are extracted from the lithium layer initially below ~4.4 V and from both the lithium and TM layers above 4.4 V.[21] During first-cycle charge, the removal of lithium from the TM

Published on 27 September 2013. Downloaded by University of Tennessee at Knoxville on 23/12/2015 15:34:36.

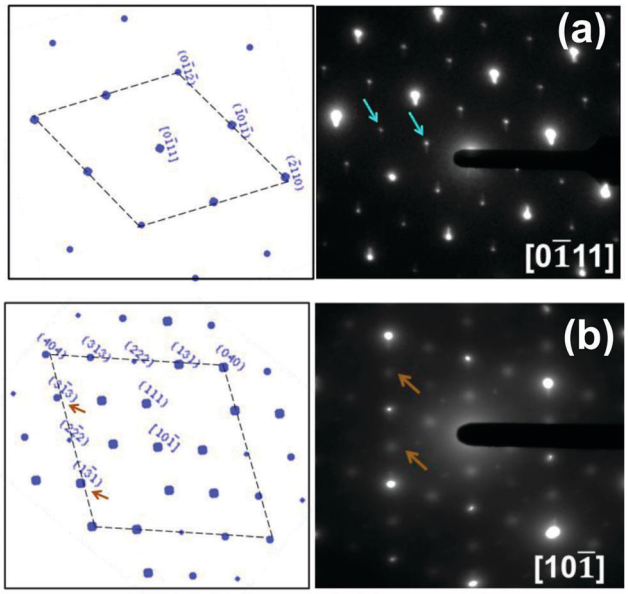

Fig. 11 SAED patterns of LMR–NMC particles cycled 125 times (a) at 4.2 V, from the [0$\bar{1}$11] zone axis in O3 lattice and (b) at 4.8 V, from the [10$\bar{1}$] spinel lattice. Simulated SAED patterns from [0$\bar{1}$11] and [10$\bar{1}$] are shown on the left side of the corresponding experimental SAED patterns.

layer (*i.e.*, Li_2MnO_3 activation) diminishes the cationic ordering in the structure. This Li_2MnO_3 activation occurs by simultaneous extraction of Li and oxygen, and is seen as a voltage plateau around 4.5 V in the charge curve. The oxygen release is an irreversible process and contributes to the irreversible capacity loss ($\sim$64 mA h g^{-1}) observed during first-cycle discharge.[10] At that point, it is reasonable to assume that there are three different types of vacancies in the LMR–NMC cathode after the first charge: (1) lithium vacancies in the lithium layer, (2) lithium vacancies in the TM layer, and (3) oxygen vacancies (Fig. 12d). In contrast only lithium vacancies form (in the lithium layer) for LMR–NMC charged at 4.2 V. During first-cycle discharge, the lithium ions should ideally go back to their respective sites to maintain the pristine structure of the LMR–NMC; however, this is not the case. After first-cycle discharge from 4.8 V, a decrease in magnetic ordering is observed, and the temperature at which bifurcation of FC and ZFC occurs in the pristine material (the T_N) slightly decreases (Table 3). Moreover, the value of the effective magnetic moment is lower than that of the pristine material. The decrease in the effective magnetic moment after one cycle was also observed for cells cycled at 4.2 V; however, the decrease is greater when the UCV is 4.8 V.

For oxide samples discharged from 4.2 V, the lower effective magnetic moment is explained by the presence of residual Ni^{3+} and lithium vacancies. For samples discharge from 4.8 V, if one assumes only 0.15 Ni^{3+} (no Ni^{2+}), then the theoretical effective magnetic moment would be 2.96 μ_B, greater than the experimental effective magnetic moment of 2.84 μ_B. The data clearly

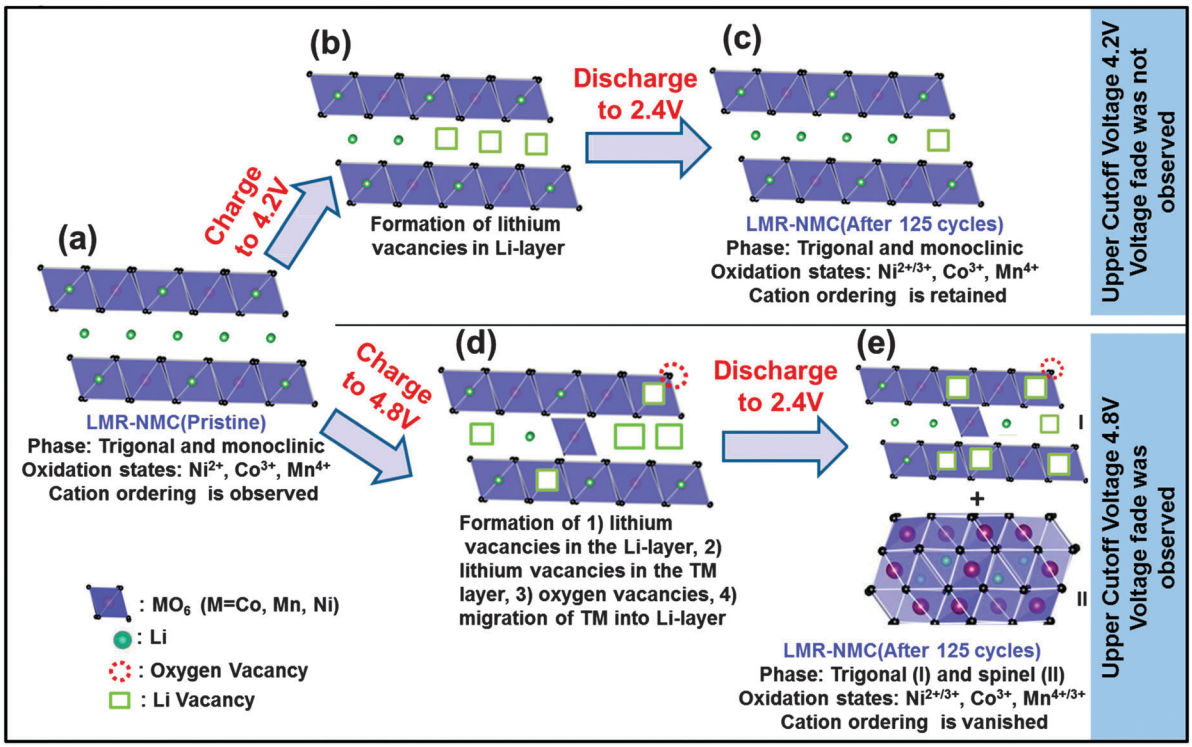

Fig. 12 Schematic of structural changes when cycling within the 2.4 V to 4.2 V window (a–b–c) and in the 2.4 V to 4.8 V window (a–d–e). (a) The pristine material has Li in the TM layer, and Co, Mn, and Ni are in 3+, 4+, and 2+ states, respectively. (b) Charging at 4.2 V, lithium vacancies are formed in the Li-layer and (c) after subsequent discharging to 2.4 V, Li vacancies are filled with Li ions and few percentage of residual Ni^{3+} with some Li vacancies after 125 cycles. (d) Charging at 4.8 V, lithium vacancies are formed in the Li layer and TM layer, oxygen vacancies are formed, and TM ion migration to Li-layer occurs. (e) Subsequent discharge after 125 cycles results the formation of both layered (I) and spinel phase (II) with Mn^{3+} ions. Voltage fade was observed when the LMR–NMC material was cycled at a cutoff voltage of 4.8 V.

 This journal is © the Owner Societies 2013

Published on 27 September 2013. Downloaded by University of Tennessee at Knoxville on 23/12/2015 15:34:36.

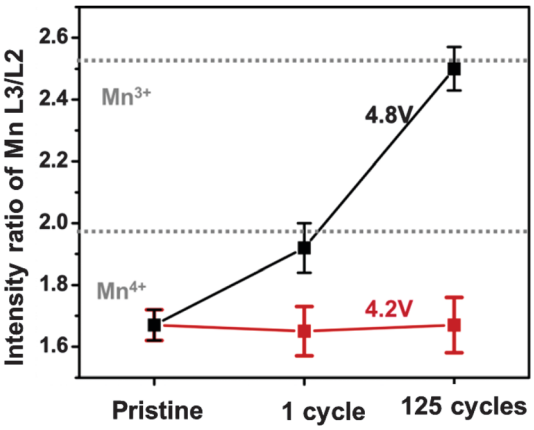

Fig. 13 Intensity ratio of Mn L3/L2 lines in pristine LMR–NMC and after 1 cycle and 125 cycles at 4.2 V and 4.8 V. The increase in the L3/L2 ratio in the particles cycled at 4.8 V for 125 cycles indicates the presence of Mn^{3+} ions.

indicate that other ions with lower magnetic moment must be present. The discharged sample should contain oxygen vacancies (generated in the voltage plateau) and for charge compensation, Mn^{2+}/Mn^{3+} and/or lithium vacancies should be present. Because the effective magnetic moment of Mn^{2+} (LS)–Mn^{3+} (LS) is less than the magnetic moment of other possible magnetic ions, we believe that these ions are responsible for reducing the effective magnetic moment.

Hence, after first discharge, the oxide structure contains some Li_2MnO_3 like areas, some Mn^{2+}/Mn^{3+} and some Ni^{3+} in addition to Li and oxygen vacancies. The presence of Mn^{3+} after the first cycle is in disagreement with the results reported by Fell *et al.*[11] based on EELS data where the authors reported only Mn^{4+} in a LMR–NMC sample ($Li[Li_{0.2}Ni_{0.2}Mn_{o.6}]O_2$), but it is in agreement with results reported by Yabuuchi *et al.*[23] where the authors report Mn^{3+} based on X-ray absorption spectroscopy data from $Li[Li_{0.2}Co_{0.13}Mn_{0.54}Ni_{0.13}]O_2$. To further extend the Fell *et al.* data comparison, EELS data were collected from Mn L-edges from representative particles in the pristine material, after 1 cycle, and after 125 cycles, at 4.2 V and 4.8 V. The intensity ratio of Mn L-edges (L3/L2) are reported in Fig. 13 (see the ESI† for the EELS spectra and intensity ratio calculation) with the values expected from Mn^{3+} and Mn^{4+}. The pristine material shows the Mn in the 4+ state; a change in the electronic state of Mn is not observed for samples cycled at 4.2 V, even after 125 cycles (in agreement with other results described above). However, when cycled at 4.8 V, the value of L3/L2 increases indicating that Mn is in the 3+ state after one cycle; this oxidation state change may result from reconstruction of the Fermi level after oxygen-ion removal in the charging process (voltage plateau) as proposed by Yabuuchi *et al.*[23] Based on previous reports[23] some percentage of TM ions (Ni^{2+}) is also expected in the lithium layer.[11,17] In this work after 10 charge–discharge cycles, cation-ordering peaks are still observed in the SAED pattern, and magnetic ordering is present in the magnetic susceptibility data. However, in SAED patterns, the intensity of the cation-ordering peaks decrease, and new spinel type reflections are observed that may arise from $A_2B_2O_4$ and/or AB_2O_4 (where A = Li, B = TM ions) type spinel compounds. The observation of spinel-phase growth upon cycling is in agreement with the previously reported *in situ* XRD results.[17,32] After 10 cycles, the presence of cation-ordering peaks in SAED patterns indicates that some fraction of the Li_2MnO_3 phase is still present, which is consistent with the magnetic-susceptibility data, where some magnetic ordering (bifurcation of FC and ZFC) is observed. Therefore, the oxide structure contains a mixture of layered hexagonal, layered monoclinic, and spinel phases. The increase in the effective magnetic moment values can be attributed to Mn^{3+} (HS) and Mn^{2+} (HS), which have the highest effective magnetic moments of the various TM ions. Mn ions in the $Li_2Mn_2O_4$ spinel are indeed in the HS configuration, and Mn in $LiMn_2O_4$ is in both HS and LS configurations. The spinel reflections and the Mn^{3+} in HS configuration indicate the formation of $Li_2Mn_2O_4$ and/or $LiMn_2O4$ spinel-like phases after 10 cycles.

After 125 cycles, the effective magnetic moment increases further, which indicates that the fraction of Mn^{3+} (HS) ions originating from $Li_2Mn_2O_4$ and/or $LiMn_2O_4$ phases increases. The Mn L3/L2 intensity ratio (Fig. 13) in the EELS data is consistent with this observation. Magnetic ordering is not seen after 125 cycles, which confirms the absence of Li-TM ordering. The SAED patterns from the [0001] zone axis also show the disappearance of cation-ordering reflections that arise from the Li_2MnO_3 regions; only reflections from the layered and spinel reflections are observed. Therefore, the LMR–NMC structure after 125 cycles is a mixture of layered trigonal and spinel phases (Fig. 12e).

In $Li_2Mn_2O_4$–$LiMn_2O_4$ spinel compounds, the Mn sublattice is in a three-dimensional network of a corner sharing tetrahedron that forms a pyrochlore lattice which is geometrically frustrated.[33,34] This frustrated behavior can be understood from the value of the factor "f" in $f = (-\theta)/T_N$,[35] where θ is the Curie–Weiss temperature and T_N is the ordering temperature. If the value of f is greater than 1, then the lattice may be regarded as being frustrated.[33,35] We calculated the f value for pristine LMR–NMC and cycled materials; the results are shown in Table 3. The maximum value of f is $\sim$1.9 (>1) for the LMR–NMC material cycled at 4.8 V for 125 cycles (Table 3) and suggests the formation of a frustrated $Li_2Mn_2O_4$–$LiMn_2O_4$ spinel lattice. However, further confirmation of this hypothesis is needed by other techniques such as magnetic-structure refinement from neutron diffraction data and frequency-dependent AC magnetic susceptibility measurements.

The mechanism of the layered-spinel transformation is still the subject of research. As reported previously for $LiNi_{0.5}Mn_{0.5}O_2$,[36,37] it is believed that the spinel transformation in LMR–NMC may occur *via* formation of an alkali atom in a tetrahedral site[14,16] during early cycling. The extraction of lithium from the TM layer (octahedral sites) may create two vacant tetrahedral sites, one in the lithium layer and another in the TM layer. Li or TM ions can then migrate to the empty tetrahedral sites to create a "Li/TM dumbbell" cell, and the structure may be an intermediate between layered and spinel phases. Over the subsequent cycles ($\sim$125 cycles in this study)

Published on 27 September 2013. Downloaded by University of Tennessee at Knoxville on 23/12/2015 15:34:36.

the nucleation and growth of the spinel phase occurs and the structure may slowly transform to the spinel phase. We are employing neutron-diffraction techniques to verify this mechanism.

Conclusion

In this study, correlation between change in cation ordering leading to structural evolution and voltage fade in an LMR–NMC cathode material was reported utilizing a combined approach of magnetic-susceptibility and TEM and the following conclusions can be drawn:

(i) Electrochemical results show that the voltage fade occurs when LMR–NMC is cycled at higher voltage (4.8 V in this study) as compared to lower voltage (4.2 V in this study).

(ii) Magnetic susceptibility and SAED patterns show cation ordering in the pristine LMR–NMC material that is retained even after 125 cycles at a cutoff voltage of 4.2.

(iii) However, the magnetic susceptibility of samples cycled at 4.8 V showed a decrease in the magnetic ordering after one cycle and eventual disappearance of magnetic ordering after 125 cycles.

(iv) The total effective magnetic moment values of TM ions decreased slightly after one cycle and remained unchanged over 125 cycles for samples cycled at 4.2 V. The decrease in the effective magnetic moment is attributed to the presence of residual Ni^{3+} and lithium vacancies in the host lattice.

(v) When the cutoff voltage is 4.8 V, the increase in the effective magnetic moment after 10 (125) cycles suggests the presence of Mn^{3+} in HS states, which may arise from a $Li_2Mn_2O_4$–$LiMn_2O_4$ spinel-type lattice.

(vi) Spinel reflections are observed in SAED patterns from particles after 10 cycles at 4.8 V. After 125 cycles, the cation-ordering peaks are not seen, and only spinel-reflections are observed along with fundamental O3 reflections.

(vii) The disappearance of cation-ordering peaks, the introduction of spinel-like reflections, and the presence of HS Mn^{3+} ions suggest that a layer to spinel-like structural rearrangement happens in the LMR–NMC oxide when cycled at a higher cutoff voltage, which may be responsible for the voltage fade in these materials.

Acknowledgements

This research at Oak Ridge National Laboratory, managed by UT Battelle, LLC, for the U.S. Department of Energy (DOE) under contract DE-AC05-00OR22725, was sponsored by the Energy Efficiency and Renewable Energy Vehicle Technologies Office (VTO) Applied Battery Research (ABR) subprogram (Program Managers: Peter Faguy and David Howell). Part of this research (magnetic measurements) was supported by the DOE Basic Energy Sciences (BES), Materials Sciences and Engineering Division and the TEM experiments by ORNL's ShaRE User Facility, which is sponsored by the DOE BES Scientific User Facilities Division. The electrodes were produced at the DOE's Cell Fabrication Facility at Argonne National Laboratory by Andrew Jansen and Bryant Polzin. The Cell Fabrication Facility is fully supported by VTO within the core funding of the ABR subprogram.

References

1 J. B. Goodenough, *J. Am. Chem. Soc.*, 2013, **135**, 1167.
2 C. Daniel, *JOM*, 2008, **60**, 43.
3 J. M. Tarascon and M. Armand, *Nature*, 2008, **451**, 652.
4 M. Hu, X. Pang and Z. Zhou, *J. Power Sources*, 2013, **237**, 229.
5 B. Xu, D. Qian, Z. Wang and Y. S. Meng, *Mater. Sci. Eng., R*, 2012, **73**, 51.
6 M. S. Whittingham, *Mater. Res. Bull.*, 2008, **33**, 411.
7 M. M. Thackeray, S.-H. Kang, C. S. Johnson, J. T. Vaughey, R. Benedek and S. A. Hackney, *J. Mater. Chem.*, 2007, **17**, 3112.
8 M. M. Thackeray, C. S. Johnson, J. T. Vaughey, N. Li and S. A. Hackney, *J. Mater. Chem.*, 2006, **15**, 2257.
9 Y. Li, M. Bettge, B. Polzin, Y. Zhu, M. Balasubramanian and D. P. Abraham, *J. Electrochem. Soc.*, 2013, **160**, A3006.
10 K. J. Carroll, D. Qian, C. Fell, S. Calvin, G. M. Veith, M. Chi, L. Baggetto and Y. S. Meng, *Phys. Chem. Chem. Phys.*, 2013, **15**, 11128, DOI: 10.1039/C3CP51927A.
11 C. R. Fell, D. Qian, K. J. Carroll, M. Chi, J. L. Jones and Y. S. Meng, *Chem. Mater.*, 2013, **25**, 1621, DOI: 10.1021/cm4000119.
12 D. Mohanty, A. S. Sefat, S. Kalnaus, J. Li, R. A. Meisner, D. P. Abraham, E. A. Payzant, D. L. Wood III and C. Daniel, *J. Mater. Chem. A*, 2013, **1**, 6249.
13 S. K. Martha, J. Nanda, G. M. Veith and N. J. Dudney, *J. Power Sources*, 2012, **199**, 220.
14 J. R. Croy, K. G. Gallagher, M. Balasubramanian, Z. Chen, Y. Ren, D. Kim, S. H. Kang, D. W. Dees and M. M. Thackeraya, *J. Phys. Chem. C*, 2013, **117**, 6525.
15 H. Yu and H. Zhou, *J. Phys. Chem. Lett.*, 2013, **4**, 1268.
16 K. G. Gallagher, J. R. Croy, M. Balasubramanian, M. Bettge, D. P. Abraham, A. K. Burrell and M. M. Thackeray, *Electrochem. Commun.*, 2013, **33**, 96.
17 D. Mohanty, S. Kalnaus, R. A. Meisner, K. J. Rhodes, J. Li, E. A. Payzant, D. L. Wood III and C. Daniel, *J. Power Sources*, 2013, **229**, 239–248.
18 H. Yu, R. Shikawa, Y.-G. So, N. Shibata, T. Kudo, H. Zhou and Y. Ikuhara, *Angew. Chem.*, 2013, **52**, 5969.
19 D. Mohanty, A. Huq, E. A. Payzant, A. S. Sefat, J. Li, D. P. Abraham, D. L. Wood and C. Daniel, *Chem. Mater.*, 2013, DOI: 10.1021/cm402278q, just accepted manuscript.
20 B. Xu, C. R. Fell, M. Chi and Y. S. Meng, *Energy Environ. Sci.*, 2011, **4**, 2223.
21 H. J. Yu, H. J. Kim, Y. R. Wang, P. He, D. Asakura, Y. Nakamura and H. S. Zhou, *Phys. Chem. Chem. Phys.*, 2012, **14**, 6584.
22 D. Mohanty, S. Kalnaus, R. A. Meisner, A. S. Sefat, J. Li, E. A. Payzant, K. Rhodes, D. Wood III and C. Daniel, *RSC Adv.*, 2013, **3**, 7479.
23 N. Yabuuchi, K. Yoshii, S.-T. Myung, I. Nakai and S. Komaba, *J. Am. Chem. Soc.*, 2011, **133**, 4404.

 This journal is © the Owner Societies 2013

Published on 27 September 2013. Downloaded by University of Tennessee at Knoxville on 23/12/2015 15:34:36.

24 T. Ohzuku, A. Ueda, M. Nagayama, Y. Iwaksihi and H. Komori, *Electrochim. Acta*, 1993, **38**, 1159.
25 D. Mohanty and H. Gabrisch, *Solid State Ionics*, 2011, **194**, 41.
26 P. Strobel and B. L. Andron, *J. Solid State Chem.*, 1988, **75**, 90.
27 N. A. Chernova, M. Ma, J. Xiao, M. S. Whittingham, J. Breger and C. P. Grey, *Chem. Mater.*, 2007, **19**, 4682.
28 D. Mohanty and H. Gabrisch, *J. Power Sources*, 2012, **220**, 405–412.
29 J. Bareνo, M. Balasubramanian, S. H. Kang, J. G. Wen, C. H. Lei, S. V. Pol, I. Petrov and D. P. Abraham, *Chem. Mater.*, 2011, **23**, 2039.
30 H. Gabrisch, R. Yazami and B. Fultz, *J. Electrochem. Soc.*, 2004, **151**, A891.
31 H. Wang, Y. Jang, B. Huang, D. R. Sadoway and Y.-M. Chiang, *J. Electrochem. Soc.*, 1999, **146**, 473.
32 A. Boulineau, L. Simonin, J. F. Colin, E. Canevet, L. Daniel and S. Patoux, *Chem. Mater.*, 2012, **24**, 3558.
33 A. S. Wills, N. P. Raju, C. Morin and J. E. Greedan, *Chem. Mater.*, 1999, **11**, 1936.
34 A. S. Wills, N. P. Raju and J. E. Greedan, *Chem. Mater.*, 1999, **11**, 1510.
35 A. P. Ramirez, *Annu. Rev. Mater. Sci.*, 1994, **24**, 453.
36 J. Breger, Y. S. Meng, Y. Hinuma, S. Kumar and K. Kang, *Chem. Mater.*, 2006, **18**, 4768.
37 H. H. Li, N. Yabuuchi, Y. S. Meng, S. Kumar, J. Bréger, C. P. Grey and Y. S-Horn, *Chem. Mater.*, 2007, **19**, 2551.